Wave Motion 46 (2009) 189–199

Contents lists available at ScienceDirect

Wave Motion

journal homepage: www.elsevier.com/locate/wavemoti

Using time-stack overlooking images to separate incident and reflected waves in wave flume

C.A. Kuo [a], H.H. Hwung [a,*], C.H. Chien [b]

[a] Department of Hydraulic and Ocean Engineering, National Cheng Kung University, Tainan 701, Taiwan
[b] NCKU Hydraulic and Ocean Engineering R&D Foundation, National Cheng Kung University, Tainan 701, Taiwan

ARTICLE INFO

Article history:
Received 12 June 2008
Received in revised form 18 October 2008
Accepted 19 November 2008
Available online 10 December 2008

Keywords:
Wave reflection
Wavenumber-frequency spectra
Time-stack overlooking image
Sloping bathymetry

ABSTRACT

A time-stack wave image technique for separating incident and reflected waves in wave flumes is presented for normally incident waves propagating over a submerged breakwater with arbitrary 2D bathymetry. The wavenumber-frequency spectra from the time-stack wave image were used to determine the directions of incident and reflected waves, and the inverse Fourier transform method was used to derive the spatial variations and the time series of incident and reflected wave. The time series of separated incident and reflected wave and the wave reflection coefficients with the various wave phases between the incident waves and the reflected waves were fairly close to the values reported by Baldock and Simmonds, and the mean deviations in this study are slightly smaller than theirs. Furthermore, according to the profile of reflected wave heights, the reflection wave heights in this study case are not the constant, due to the incident waves encounter the various structures and sloping bathymetry. Additionally, existing 2D methods for separating incident and reflected waves over the sloping bathymetry; the water depths at the wave gauges must be known in order to calculate the linear shoaling coefficients. The present method, in contrast, does not require knowledge of the water depth, making it more practical than existing methods.

1. Introduction

In general, most marine structures or protected works are arranged on a sloping bathymetry. When the wave trains pass through the marine structures or protected works, the phenomenon of wave reflection will occur, and this profoundly affects the hydrodynamics and sediment transport in front of the reflector. Over the past five decades, many methods have been presented to estimate the reflection coefficient for 2D waves propagating over a horizontal bed. Healy [1] used the maximum and minimum of the standing wave envelope to estimate the reflection coefficients of regular waves. Goda and Suzuki [2] presented a frequency domain method to estimate the reflection coefficients of irregular waves. Mansard and Funke [3] improved Goda and Suzuki's method [2] using a least squares algorithm. Frigaard and Brorsen's method [4] was based on the use of digital filters and can separate the wave field in real time to present a method for separating incident and reflected irregular waves in a 2D wave field. Suh et al. [5] developed a technique to separate the incident and reflected waves propagating on a known current in a laboratory wave–current flume by analyzing wave records measured at two or more locations using a least squares method.

The above-mentioned methods are frequently used to calculate the wave reflection coefficients from a beach or marine structure. However, none of these methods is suitable to estimate the reflection coefficients for waves propagating over a

* Corresponding author. Tel.: +886 6 3840207; fax: +886 6 3840206.
E-mail address: hhhwung@mail.ncku.edu.tw (H.H. Hwung).

0165-2125/$ - see front matter
doi:10.1016/j.wavemoti.2008.11.003

sloping bed or an arbitrary bathymetry. Recently, Baldock and Simmonds [6] took the effect of linear shoaling, which is used to determine the amplitude and phase change between two measurement positions, into account to modify Frigaard and Brorsen's method [4]. Their method is able to separate the incident and reflected waves over a bed with arbitrary 2D bathymetry. In addition, Chang and Hsu [7] provided a frequency-domain method for estimating incident and reflected waves in the case of normally incident waves propagating over a sloping beach in a wave flume. In this method, the linear wave shoaling is applied to determine wave amplitudes and phases due to variations of the bathymetry, and the wave reflection coefficient is estimated using wave heights measured at two fixed wave gauges. These two methods are developed from the linear wave shoaling theory. The water depths at the wave gauges must be known in order to calculate the linear shoaling coefficients. Furthermore, the existing methods cannot separate the spatial variations and the time series of incident and reflected waves at a time.

In this study three CCD cameras were arranged at the side of the wave flume to record the wave images to extend the view of wave motion for the subsequent separation of incident and reflected wave profiles. Image processing techniques, such as geometrical calibration, image merging, and edge detection, were used to combine the images of the wave profiles from the three CCD cameras and to extract the time series data of the wave profile. Next, all of the time series data of the wave profiles were composed as a time-stack wave image, and the k-σ spectrum from the time-stack wave image was used to determine the directions of incident and reflected waves. Finally, the inverse Fourier transform method was applied to derive the time series of incident and reflected wave profiles. The results were compared with linear wave shoaling theory and with the method of Baldock and Simmonds [6] in order to validate the feasibility of the present technique. Furthermore, according to the results of separated incident and reflected waves, characteristic wave height profiles of incident and reflected waves were studied.

2. Experimental setup

The physical model tests were carried out in a 2D wave flume with a length of 100 m, a width of 3 m, and a depth of 3.2 m in the Department of Hydraulic and Ocean Engineering, National Cheng Kung University. In this study, the layout of the bathymetry profile, which was based on Fan-Zih-Lun coast at Ping-Tung in Taiwan, was installed in the flume with a physical model scale of 1/20. In addition, a submerged breakwater was positioned at a depth of approximately 25 cm. The experimental water depth was kept at 188 cm in the constant depth section.

To extend the wave monitoring range in the tests, three CCD video cameras (SHOWCASE K-ZC231N) with a capture rate of 25 images per second and an image resolution of 640 dpi (H) $\times$ 480 dpi (V) were set at the side of the wave flume to capture the water surface from above. According to the study by Kuo et al [8] of wave profile measurement from cameras placed overhead, the overhead angle of CCD images for wave profile measurement should be smaller than 45° because an angle greater than 45° would lead to higher analysis error. Therefore, the overlooking posture angle of CCD video cameras was set to approximately 15° in this study. To compare the wave series data that were identified from the CCD images, the capacitance wave gauges with a resolution of 2 mm were placed at x = 520 and 780 cm to measure the water surface at a sampling rate of 25 Hz. A detailed schematic diagram of the experimental flume and instrumentation in this study is shown in Fig. 1.

3. Image processing and wave data verification

3.1. image rectification and reconstruction

During the measuring process, the captured images of the CCD camera would usually be distorted due to the curvature of the CCD camera's lens; this leads to deviations of the measured results. Thus, the geometric calibration of CCD camera is very important for measuring water surfaces. Recently, several calibration algorithms were proposed, including the famous DLT (Direct Linear Transform) algorithm, Tasi's algorithm, and Zhang's algorithm [9–11]. In general, the camera properties can be described using a pinhole camera model. Fig. 2 shows a schematic diagram of the pinhole camera model. Under perspective projection, a 3D point M in space is projected to an image point m via a 3×4 rank 3-projection matrix P as:

$$\lambda m = PM = A_{3\times3}[R_{3\times3}, t_{3\times1}]M \tag{1}$$

where m is the image coordinate system; M is the world coordinate system; λ is a non-zero scalar, and R and t, called the extrinsic parameters, are the rotation and translation that relate the world coordinate system to the camera coordinate system. A, called the camera intrinsic matrix, can be defined as:

$$A_{3\times3} = \begin{bmatrix} f_u & \gamma & u_0 \\ 0 & f_v & v_0 \\ 0 & 0 & 1 \end{bmatrix} \tag{2}$$

where f_u, f_v represent the camera's focal length corresponding to the u and v axes of camera coordinates; (u_0, v_0) are the coordinates of the camera's principal point; γ refers to the skew factor. Then, the Eq. (1) can be expressed as Eq. (3).

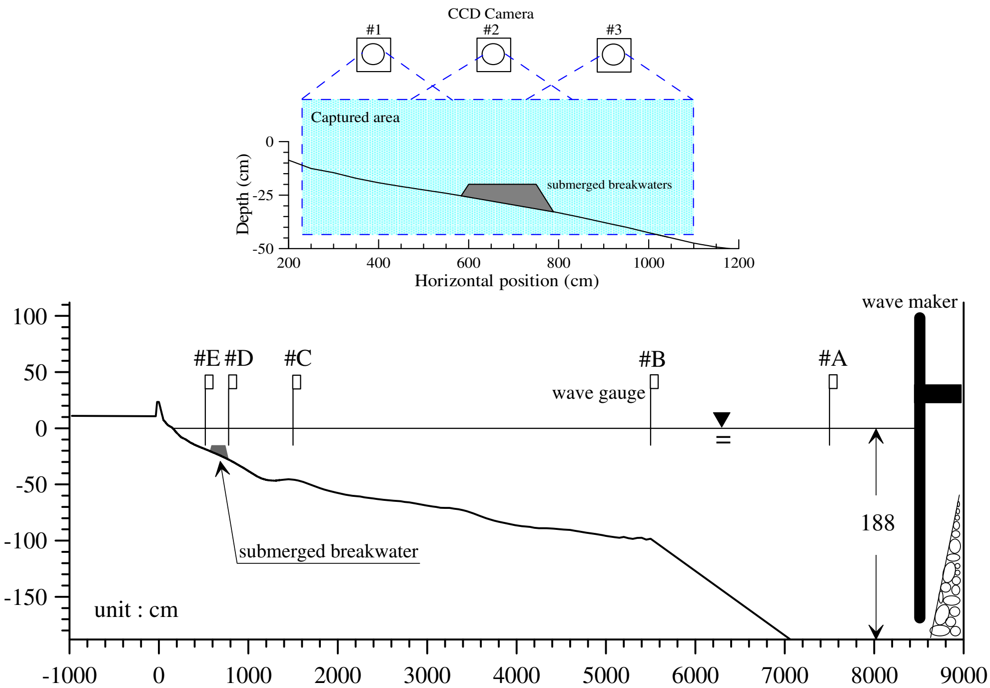

Fig. 1. Schematic diagram of experimental wave flume and instrumentation.

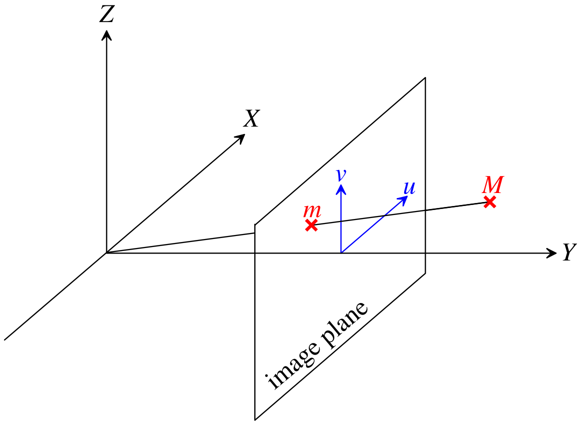

Fig. 2. Schematic diagram of pinhole camera model.

$$\begin{bmatrix} x_1 \\ x_2 \\ x_3 \end{bmatrix} = A_{3\times 3}[R_{3\times 3}, t_{3\times 1}] \begin{bmatrix} X \\ Y \\ Z \\ 1 \end{bmatrix} = \begin{bmatrix} p_{11} & p_{12} & p_{13} & p_{14} \\ p_{21} & p_{22} & p_{23} & p_{24} \\ p_{31} & p_{32} & p_{33} & p_{34} \end{bmatrix} \begin{bmatrix} X \\ Y \\ Z \\ 1 \end{bmatrix} \tag{3}$$

According to Eq. (3), the relationship of *X*-*Z* planar projective transformation between image coordinates and world coordinates can be rearranged as in Eq. (4).

$$\begin{cases} \frac{x_1}{x_3} = u = \frac{p_{11}X + p_{13}Z + p_{14}}{p_{31}X + p_{33}Z + p_{34}} \\ \frac{x_2}{x_3} = v = \frac{p_{21}X + p_{23}Z + p_{24}}{p_{31}X + p_{33}Z + p_{34}} \end{cases} \tag{4}$$

Eq. (4) is homogeneous. Thus, p_{34} can be assumed to be 1 for solving the parameters of planar projective transformation. Then, Eq. (4) can be rearranged as

$$\begin{bmatrix} X & Z & 1 & 0 & 0 & 0 & -uX & -uZ \\ 0 & 0 & 0 & X & Z & 1 & -vX & -vZ \end{bmatrix} [h] = \begin{bmatrix} u \\ v \end{bmatrix} \tag{5}$$

where h is the matrix of planar projective transformation and is described in Eq. (6). With at least four known points, the matrix of planar projective transformation (h) can be determined by a least squares algorithm.

$$[h] = [P_{11} \quad P_{12} \quad P_{14} \quad P_{21} \quad P_{22} \quad P_{24} \quad P_{31} \quad P_{32}]^T \tag{6}$$

The phenomenon of radial lens distortion can occur in images taken by a CCD camera. The displacement due to radial lens distortion can be rectified using Eq. (7), according to Holland et al. [12].

$$\sqrt{(u_d - u_0)^2 + (v_d - v_0)^2} - \sqrt{(u_p - u_0)^2 + (v_p - v_0)^2} = k_3 r^3 + k_1 r \tag{7}$$

where k_1 and k_3 are distortion coefficients, (u_p, v_p) are the ideal image coordinates, (u_d, v_d) are the distorted image coordinates, and r is the distance from the image center (u_0, v_0) to the point of distortion image (u_d, v_d). Among them, the ideal image coordinates (u_p, v_p) can be calculated through Eq. (5), after the matrix of planar projective transformation (h) is determined.

As the parameters of the matrix of planar projective transformation and radial distortion are determined, the resolution of each pixel in the horizontal and vertical directions can be obtained from the relationship between image coordinates and world coordinates. Then, the planar projective image at the true scale can be reconstructed using the bilinear interpolation method [8,13]. The bilinear interpolation is defined as

$$I(u', v') = b_1 u' + b_2 v' + b_3 u' v' + b_4 \tag{8}$$

where u' and v' are the planar projective image coordinates of the actual scaling and b_1, b_2, b_3, and b_4 are the transformed coefficients of the pixel's intensity. In addition, to reduce the lost image information or overexpansion in the processing of the bilinear image interpolation, the planar projective image of the actual scaling was controlled to 640×480 pixels.

3.2. Image merging

Through the above processes, the relationship between the image coordinates and world coordinates in each frame of the different cameras can be obtained. Kuo and Chien's method [13] was used to combine images from the different cameras to obtain the improved effects of merging images. In Kuo and Chien's method [13], the feature sub-image that includes the physical control points in the area of overlap between two-neighbor rectification images is selected first. Then the cross-correlation values of feature sub-images in two-neighbor rectification images are calculated, and the position of maximum cross-correlation value is found as the image matching point. Finally, the frames of the different cameras can be merged by aligning the image matching points. Fig. 3 shows the merged image of a wave profile with H_o = 13.1 cm and T_o = 2.0 sec.

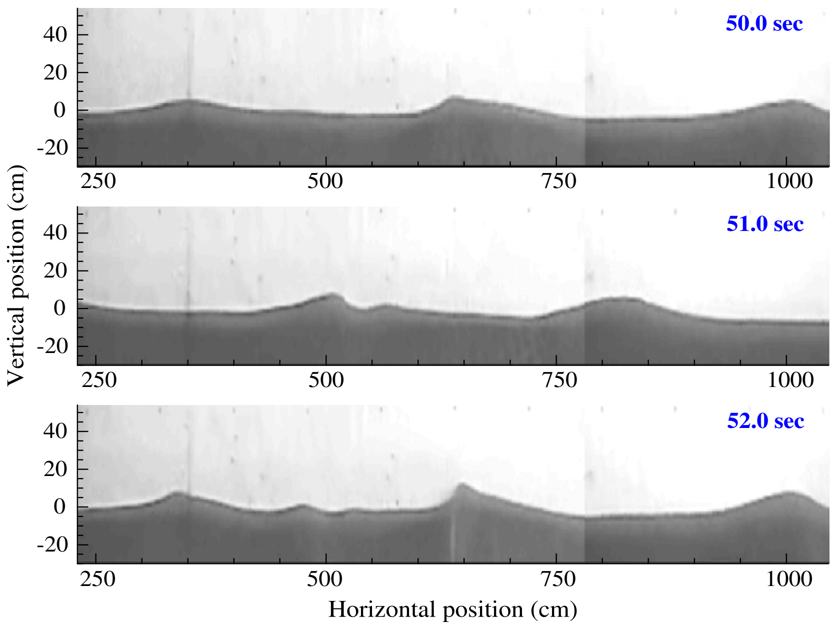

Fig. 3. The merged image of a wave profile with H_o = 13.1 cm and T_o = 2.0 sec.

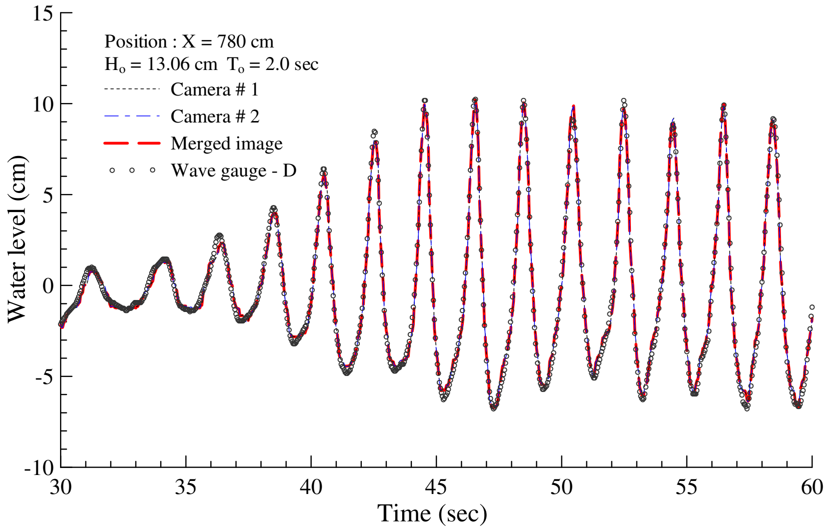

Fig. 4. Time series of water surface with H_o = 13.1 cm and T_o = 2.0 sec at x = 780 cm from the camera #1 images, camera #2 images, merged images, and the wave gauge (D).

The wave profiles of the merged image were fairly smooth, and the wave surface in the overlap area of two-neighbor images is continuous.

3.3. Wave extraction and verification

All merged images of the wave series in each horizontal position were analyzed, using the "time-stack" method described by Aagaard and Holm [14]. As the time-stack wave images in each horizontal position were created, their pixel intensity distributions were calculated to determine the threshold value between water and side flume using Otsu's algorithm [15]. Then, the wave series in each horizontal position could be detected and extracted on the basis of this threshold value.

Fig. 4 shows the time series of water surface with H_o = 13.1 cm and T_o = 2.0 sec at x = 780 cm from the images of camera 2, camera 3, the merged images, and the wave gauge (D). Fig. 5 shows the time series of water surface with H_o = 13.1 cm and T_o = 2.0 sec at x = 520 cm from the images of camera 1, camera 2, the merged images, and wave gauge (E). The results show that the water surface in the merged images agrees with the surface as seen in the unmerged images. The time series of waves in the image analyses were close to the records from the wave gauges. According to Table 1, the deviations of wave

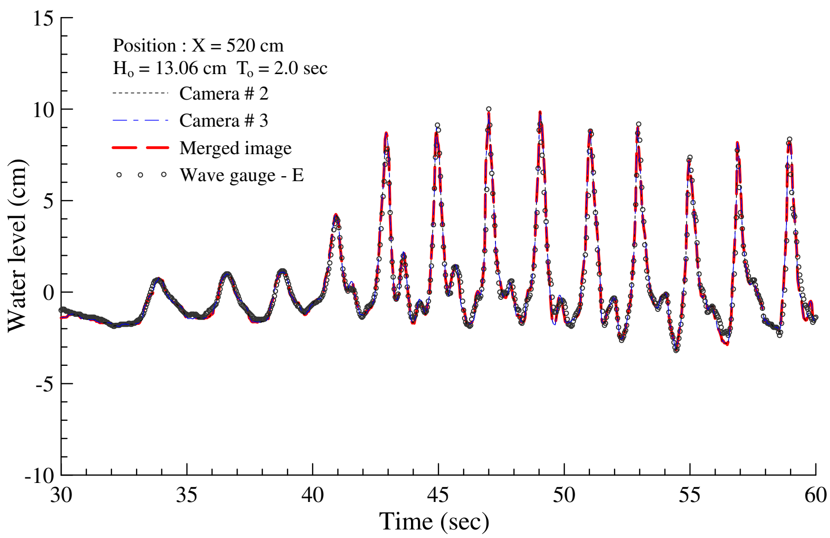

Fig. 5. Time series of water surface with H_o = 13.1 cm and T_o = 2.0 sec at x = 520 cm from the images of camera 2, camera 3, merged images, wave gauge (E).

Table 1
Wave height and period with H_o = 13.1 cm and T_o = 2.0 sec from the camera images, merged images, and wave gauges.

x (cm)	Term	Wave height (cm)	Wave period (sec)
780	Camera 1	15.49	2.00
	Camera 2	15.46	2.00
	Merged image	15.49	2.00
	Wave gauge (D)	15.64	2.00
520	Camera 2	12.18	2.04
	Camera 3	12.17	2.00
	Merged image	12.17	2.04
	Wave gauge (E)	12.37	2.02

height and period between the merged images and the wave gauges are fairly small (0.15-0.2 cm and 0-0.02 sec, respectively) and lie within the wave gauge's accuracy. Therefore, the results of merged images can be applied to further studies.

4. Method for separating incident and reflected waves

Fig. 6 shows the time-stack image of waves transmitted over the submerged breakwater. The incident and reflected waves can be seen clearly in the time-stack image. To separate the incident and reflected waves in the wave flume, the

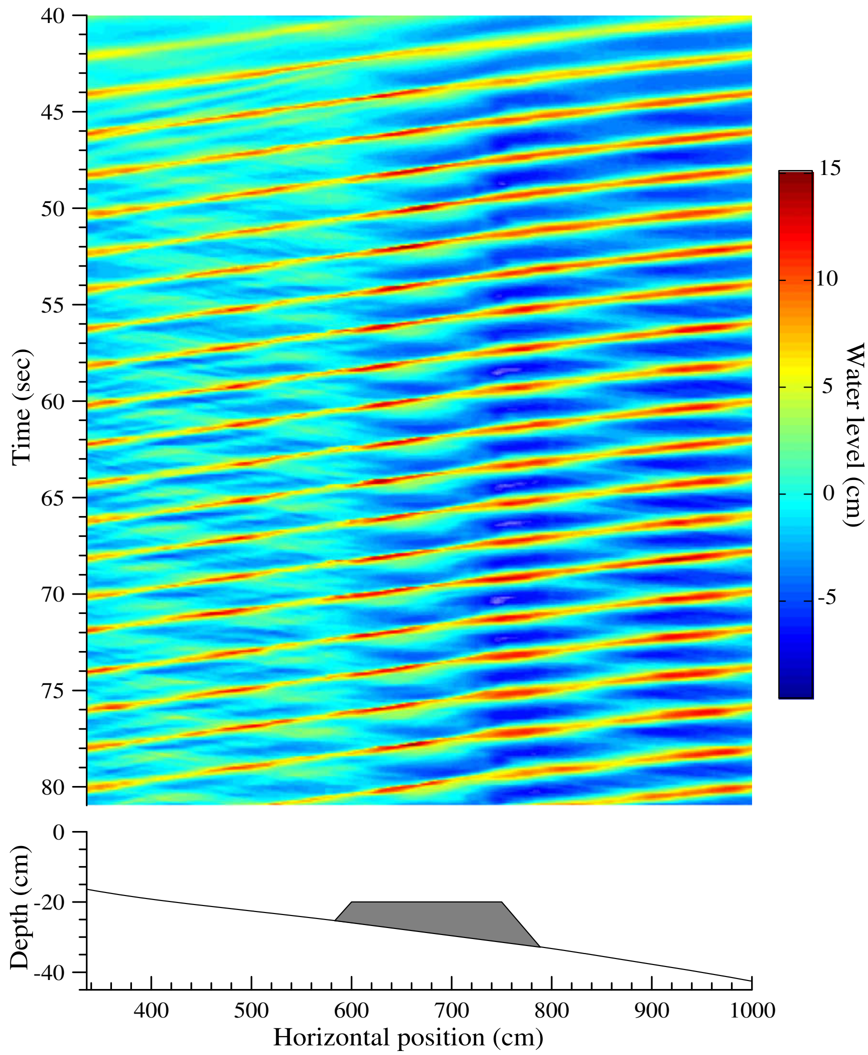

Fig. 6. Time-stack wave image of waves transmitted over a submerged breakwater.

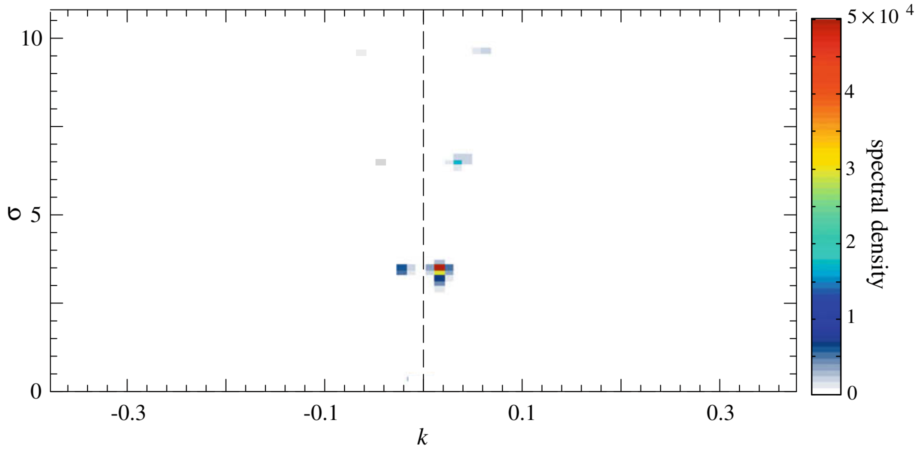

Fig. 7. k-σ spectrum from the time-stack image.

time-stack image was assumed to be a 2-D spatial image. Then, the 2-D spatial Fourier transform algorithm is used to calculate the k-σ spectra from the time-stack image ($N \times N$ pixels). A 2-D Fourier coefficient is defined as

$$\eta(k,\sigma) = \frac{1}{N^2} \sum_{x=-N/2+1}^{N/2} \sum_{t=-N/2+1}^{N/2} \eta(x,t) \exp[-i(kx+\sigma t)] \tag{9}$$

where x is the position of time-stack image in the horizontal axis and t is time. $\eta(x,t)$ is the height of the wave surface. k is the wavenumber, and σ is the angular frequency. In this study, N was set to 1024 (2^{10}). The horizontal range (x) of separated incident and reflected waves was set from 335 cm to 1000 cm, and the analysis time was set from 40 sec to 80.96 sec.

The k-σspectrum (φ) of the time-stack image can be derived from Eq. (10), and the wave velocity ($\vec{C}$) can be defined by Eq. (11). Fig. 7 shows the k-σ spectrum of the time-stack image. In this study, the tests were carried out in a 2-D wave flume, and the horizontal position was set from the left side to the right side. Therefore, if the wave velocity was negative, the wave direction was defined as onshore. If the wave velocity was positive, the wave direction was defined as offshore. Next, because the wave directions were known, the inverse Fourier transform method was used to separate the spatial variations and the

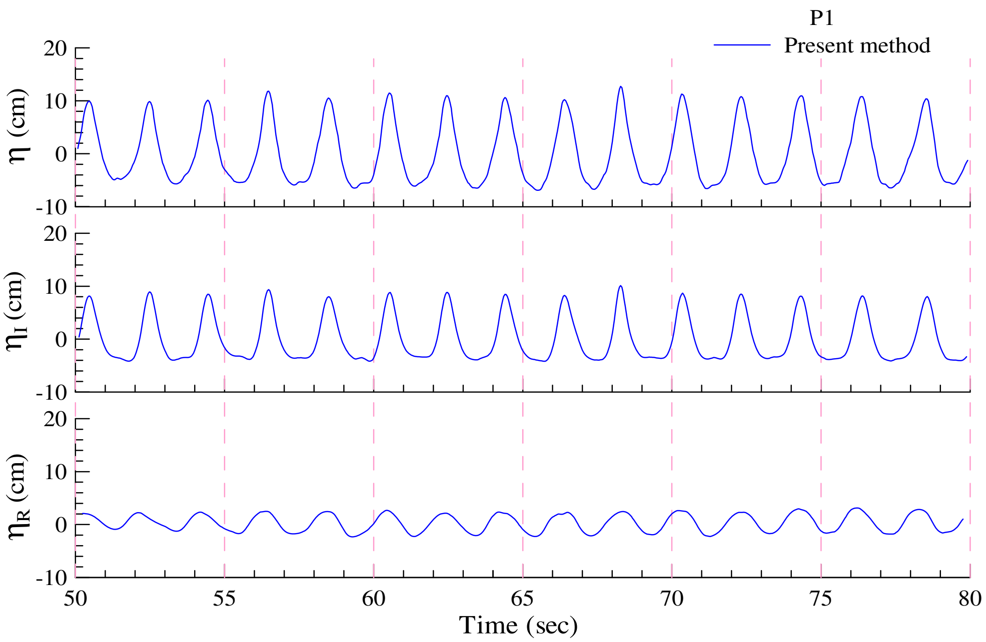

Fig. 8. Time series of separated incident and reflected waves at x = 893.1 cm from Fig. 6.

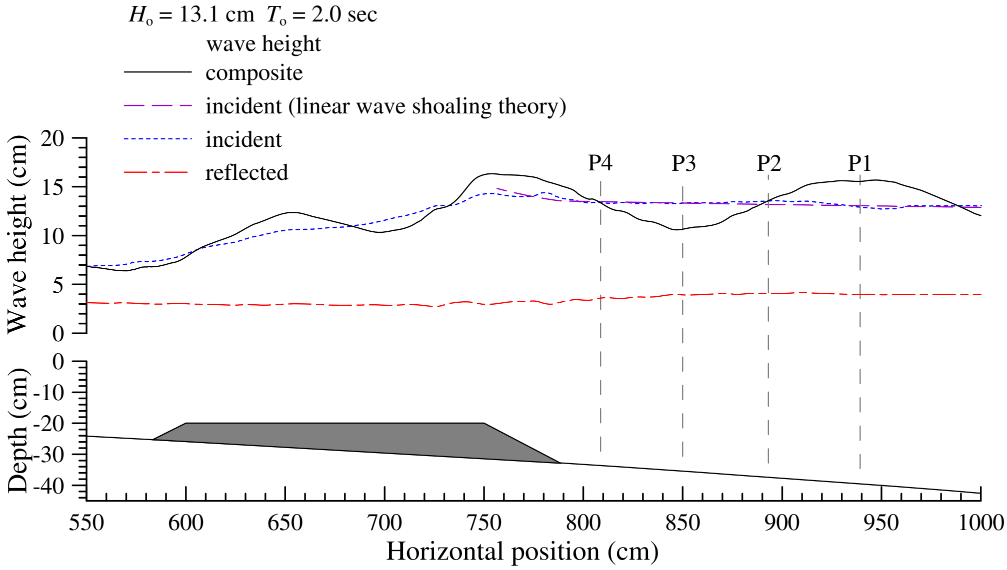

Fig. 9. The wave height profiles of composite waves, incident waves, and reflected waves in Fig. 6.

time series of incident and reflected waves, such as Eq. (12a) and Eq. (12b), respectively. Fig. 8 shows the time series of separated incident and reflected waves at $x = 893.1$ cm in Fig. 6.

$$\phi(k,\sigma) = |\eta(k,\sigma)|^2 \tag{10}$$

$$\vec{C} = \frac{\sigma}{k} \tag{11}$$

$$\eta_I(x,t) = \sum_k \sum_\sigma \eta_I(k,\sigma)\exp[i(kx+\sigma t)] \quad \text{if } \vec{C} > 0 \tag{12a}$$

$$\eta_R(x,t) = \sum_k \sum_\sigma \eta_R(k,\sigma)\exp[i(kx+\sigma t)] \quad \text{if } \vec{C} < 0 \tag{12b}$$

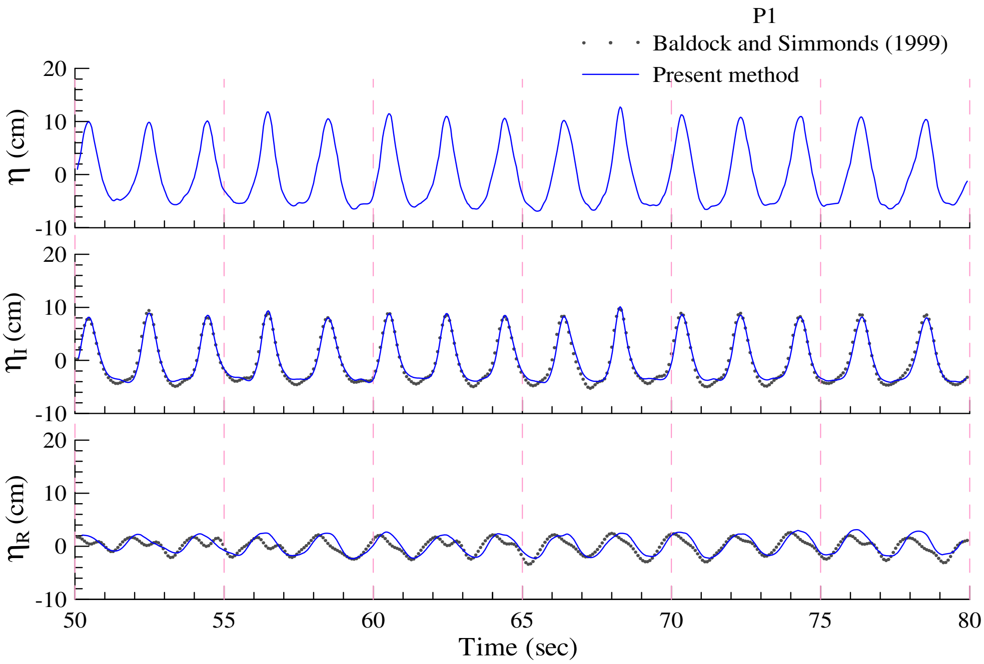

Fig. 10. Time series of separated incident and reflected waves at P1 with H_o = 13.1 cm and T_o = 2.0 sec.

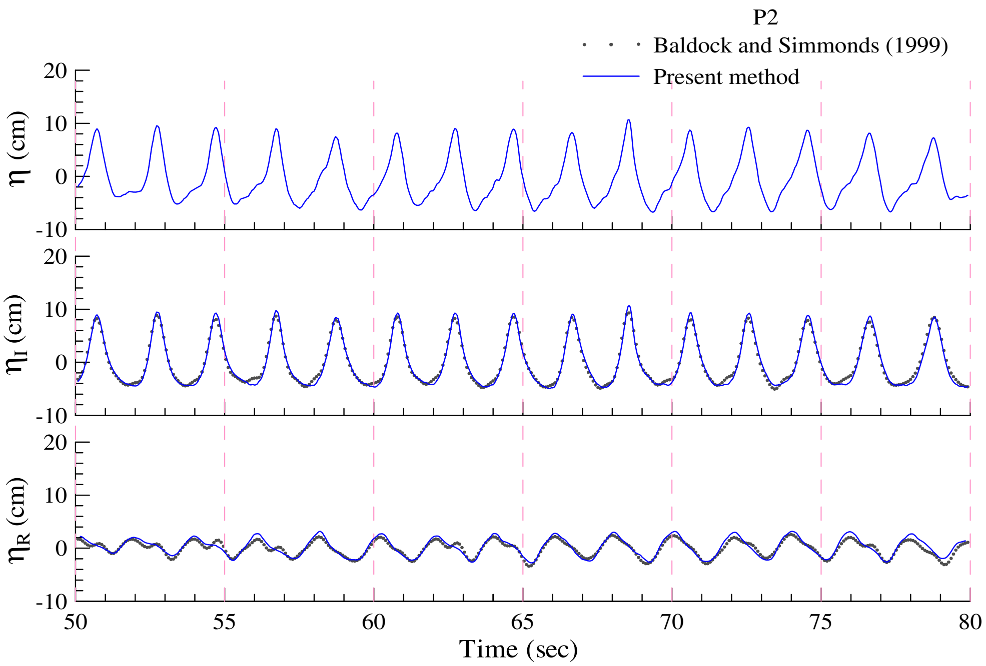

Fig. 11. Time series of separated incident and reflected waves at P2 with H_o = 13.1 cm and T_o = 2.0 sec.

5. Sample results and discussion

The k-σ spectra from the time-stack wave image was used to determine the directions of incident and reflected waves, and the inverse Fourier transform method was used to calculate the spatial variations and the time series of incident and reflected wave. This allowed the wave height profiles of incident and reflected waves to be derived. Fig. 9 shows the wave height profiles of composite, incident, and reflected waves with H_o = 13.1 cm and T_o = 2.0 sec over a submerged breakwater

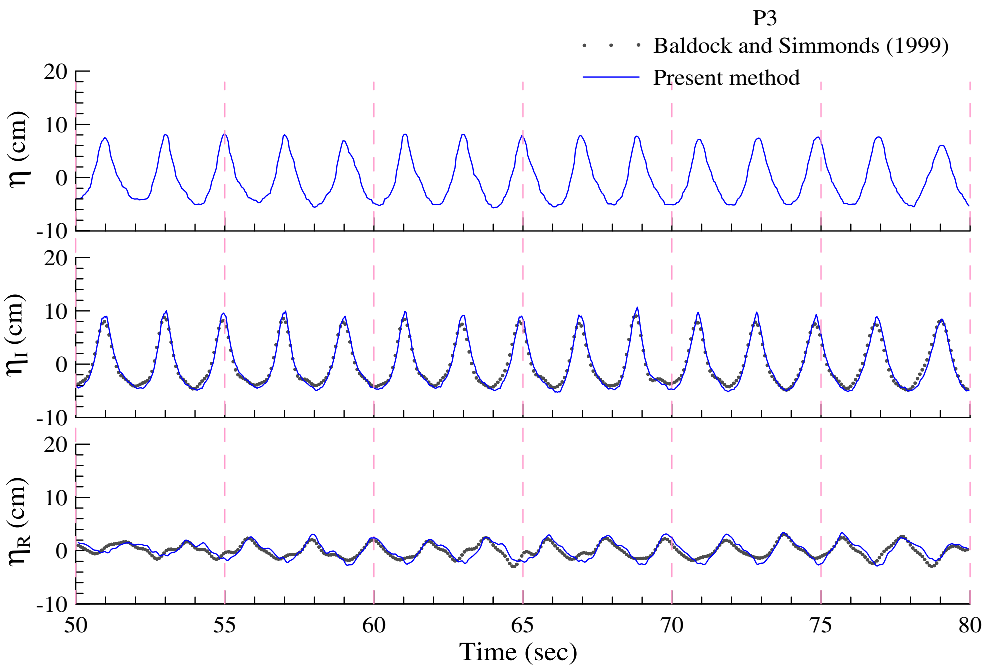

Fig. 12. Time series of separated incident and reflected waves at P3 with H_o = 13.1 cm and T_o = 2.0 sec.

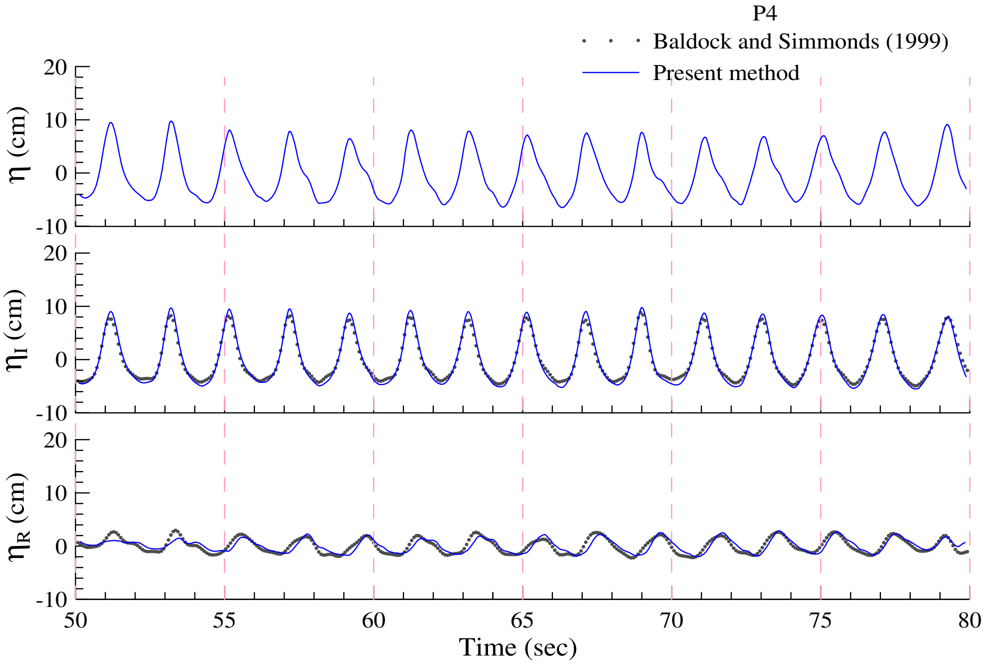

Fig. 13. Time series of separated incident and reflected waves at P4 with H_o = 13.1 cm and T_o = 2.0 sec.

Table 2
The wave heights, wave reflection coefficients, and mean deviations.

Method	Analysis term	P1	P2	P3	P4
Linear wave shoaling theory	H_I (cm)	13.06	13.21	13.28	13.47
Baldock and Simmonds (1999)	H_I (cm)	13.02	13.18	12.69	12.51
	H_R (cm)	4.11	4.06	3.89	3.48
	H_C (cm)	15.89	13.58	10.46	13.11
	kr	0.32	0.31	0.31	0.28
	$\overline{\eta-(\eta_I+\eta_R)}$(cm)	0.27	0.45	0.51	0.38
Method described here	H_I (cm)	12.89	13.56	13.35	13.28
	H_R (cm)	4.05	4.02	3.95	3.58
	H_C (cm)	15.53	13.60	10.67	13.35
	kr	0.31	0.30	0.30	0.27
	$\overline{\eta-(\eta_I+\eta_R)}$(cm)	0.25	0.37	0.43	0.33

with arbitrary 2D bathymetry. To compare with the linear wave theory, the wave height profiles of incident waves in linear wave shoaling theory in front of the submerged breakwater are also shown in Fig. 9.

In Fig. 9, the trend of incident wave heights of separated waves in front of x = 750 cm agreed with the heights predicted by linear wave shoaling theory. The submerged breakwater had the effect of decreasing the height of incident waves and causing the waves to be transmitted over the top of the breakwater. The reflected wave heights for x = 600 cm to 750 cm remained approximately 2.90-3.12 cm due to the effects of the seawall and the bathymetry between the sea wall and the submerged breakwater. However, from the front slope of the submerged breakwater to x = 850 cm, the reflected wave heights gradually increased. While x was greater than 850 cm, the reflected wave heights remained between 3.95 and 4.18 cm. Consequently, the reflection wave heights in this study case are not the constant, due to the incident waves encounter the various structures and sloping bathymetry.

To verify the results of using the present method to separate incident and reflected waves in Fig. 11, the time series of separated incident and reflected waves at P1, P2, P3, and P4 with various wave phases between the incident waves and the reflected waves (0, π/2, π and 3π/2, respectively) were compared with those predicted by linear wave shoaling theory and by the method of Baldock and Simmonds [6]. According to Figs. 10–13, the present method calculated time series of separated incident and reflected waves at P1, P2, P3 and P4 with phase differences that agreed with those reported by Baldock and Simmonds [6]. Table 2 shows that the incident wave heights at P1, P2, P3, and P4 calculated by the present method were close to those predicted by Baldock and Simmonds [6] and by linear wave shoaling theory. The reflected wave heights also were similar to those of Baldock and Simmonds [6]. Furthermore, the wave reflection coefficients at P1, P2, P3, and P4 from the present method agree with the results of Baldock and Simmonds [6]. In addition, Table 2 shows that the mean deviations $(\overline{\eta_s - (\eta_I + \eta_R)})$ at P1, P2, P3, and P4 calculated by the present method are approximately 0.25-0.43 cm, which are slightly smaller than those of Baldock and Simmonds [6].

According to above analysis, the presented method for separating incident and reflected waves in regular waves has a well result. The development of presented method for separating incident and reflected waves is based on the concept of k-σspectra from the time-stack wave image. The wave direction is determined by the various components of k and σ. Then, the spatial variations and the time series of incident and reflected waves are calculated by the inverse Fourier transform theory. Furthermore, the scatters of k and σ spectra in random waves would just be more continuous and wider than those in regular waves. Hence, the presented method can be used to separate incident and reflected waves in random waves.

6. Conclusions

In this study, a time-stack wave image technique for separating incident and reflected waves in a wave flume is presented for normally incident waves propagating over a submerged breakwater with arbitrary 2D bathymetry. The k-σ spectra from the time-stack wave image was used to determine the directions of incident and reflected waves, and the inverse Fourier transform method was applied to derive the spatial variations and the time series of incident and reflected wave. To validate the feasibility of the present technique, the results of separated incident and reflected waves were compared with those predicted by linear wave shoaling theory and with the method of Baldock and Simmonds [6]. The results show that the present method determined incident wave heights with various phase differences (0, $\pi/2$, π and $3\pi/2$) that were close to those presented by Baldock and Simmonds [6] and to those predicted by linear wave shoaling theory. The reflected wave heights were similar to those reported by Baldock and Simmonds [6]. The time series of separated incident and reflected waves and the wave reflection coefficients agreed with those of Baldock and Simmonds [6], while the mean deviations $(\overline{\eta_s - (\eta_I + \eta_R)})$ in this study were slightly smaller than theirs.

Additionally, the development of presented method for separating incident and reflected waves in this study is based on the concept of k -σspectra from the time-stack wave image. The scatters of k -σspectra in random waves would just be more continuous and wider than those in regular waves. Hence, the presented method can be used to apply for separating incident and reflected waves in random waves.

Several 2D methods for separating incident and reflected waves over a sloping bathymetry have been developed from linear wave shoaling theory, including those of Baldock and Simmonds [6] and of Chang and Hsu [7]. In these models, the water depths at the wave gauges must be known in order for the linear shoaling coefficients to be calculated. The present method, in contrast, does not require knowledge of water depth, making it more practical than existing methods.

References

[1] J.J. Healy, Wave damping effect of beaches, Proc. Int. Hydraulics Convention 1 (1952) 213–220.
[2] Goda Y., Suzuki Y. Estimation of incident and reflected waves in random wave experiments. in: Proc. 15th Int. Conf. on Coastal Eng., ASCE, (1976), pp. 828-845.
[3] Mansard E.P.D., Funke E.R., The measurement of incident and reflected spectra using a least squares method, in: Proc. 16th Int. Conf. on Coastal Eng., ASCE, (1980), pp. 154-172.
[4] P. Frigaard, M. Brorsen, A time domain method for separating incident and reflected irregular waves, Coastal Engineering 24 (1995) 205–215.
[5] K.D. Suh, W.S. Park, B.S. Park, Separation of incident and reflected waves in wave-current flumes, Coastal Engineering 43 (2001) 149–159.
[6] T.E. Baldock, D.J. Simmonds, Separation of incident and reflected waves over sloping bathymetry, Coastal Engineering 38 (1999) 167–176.
[7] H.K. Chang, T.W. Hsu, A two-point method for estimating wave reflection over a sloping beach, Ocean Engineering 30 (2003) 1833–1847.
[8] Kuo CA, Chien CH, Lee MC. Wave profile measurement by the overlooking capture in wave flume. In: PACON 2005, (2005), pp. 21-32.
[9] Abdel-Aziz Y.I., Karara H.M., Direct linear transformation from comparator coordinates into object space coordinates in close range photogrammetry, in: Proc. of the ASP/UI Symposium, Close-Range Photogrammetry, (1971), pp. 1-18.
[10] R.Y. Tsai, A versatile camera calibration technique for high-accuracy 3D machine vision metrology using off-the-sheff TV cameras and lenses, IEEE J. of Robotics and Automation 3 (1987) 323–344.
[11] Z. Zhang, A flexible new technique for camera calibration, IEEE Transactions on Pattern Analysis and Machine Intelligence 22 (2000) 1330–1334.
[12] K.T. Holland, R.A. Holman, T.C. Lippmann, J. Stanley, N. Plant, Practical use of video imagery in nearshore oceanographic field studies, IEEE Journal of Oceanic Engineering 22 (1997) 81–92.
[13] Kuo CA, Chien CH. Extending of view range in wave flume by image merging technique, in: Proc. 16th Conf. on Hydraulic Engineering in Taiwan, (2007), pp. 859-865. (In Chinese).
[14] T. Aagaard, J. Holm, Digitization of wave run-up using video records, Journal of Coastal Research 5 (1989) 547–551.
[15] N. Otsu, A threshold selection method from gray level histogram, IEEE Trans. on System, Man, and Cybernetics. 8 (1978) 62–66.